A Novel Grid-forming Voltage Control Strategy for Supplying Unbalanced Microgrid Loads Using Inverter-based Resources

Bei Xu, Victor Paduani, Hui Yu, David Lubkeman, Ning Lu
FREEDM Systems Center, *Department of Electrical and Computer Engineering*
North Carolina State University, Raleigh, NC
{bxu8, vdaldeg, hyu11, dllubkem, nlu2}@ncsu.edu

***Abstract*—This paper presents a novel grid-forming voltage control strategy for a battery energy storage system to maintain balanced three-phase output voltages when serving unbalanced loads. A stationary reference frame ($\alpha\beta$) based control scheme is proposed to regulate positive-sequence and negative-sequence voltages. Compared with the conventional rotating reference frame (dq) based control scheme, the proposed scheme shows better dynamic performance. Then, we analyze the system zero-sequence network and propose adding a grounding transformer to the Y/Yg connected output transformer to further reduce the voltage unbalance at the point of common coupling. The simulation results demonstrate the effective performance of the proposed voltage control scheme. Based on the results, the power-voltage unbalance curve is derived for different output transformer configurations to establish the relationship between the power unbalance limit and the voltage unbalance limit for microgrid power scheduling.**

***Index Terms*—Grid-forming, three-phase battery inverter, transformer, unbalanced load, voltage control.**

I. Introduction

Grid-forming inverter-based resources (IBRs) are critical for regulating voltage and frequency while responding to frequent load fluctuations in off-grid, microgrid operation. One distinct operational requirement in distribution system operation is to serve unbalanced loads. When delivering unbalanced three-phase load currents, the non-zero internal impedance of an IBR leads to unbalanced voltages at the point of common coupling (PCC). However, severely unbalanced system voltage in steady-state or during transients can cause damages or deteriorated operation to many voltage-sensitive loads, for example, three-phase motor loads [1].

In the literature, there are two general considerations when designing grid-forming IBRs for balancing system voltage: topology and control. Inverter topology design has three developed typologies: three-phase three-leg inverter with split dc-link capacitors, three-phase four-leg inverter [2], and three-phase combined inverter [3]. The second topology and corresponding control strategies are complex and not suitable for the system that needs an isolation transformer. The third topology consists of three single-phase inverters, which is mostly used in residential low-power applications. Thus, in this paper, we focus on the three-phase, three-leg inverter topology for grid-forming voltage regulation because this topology is commonly used by manufacturers and is suitable for high-power applications.

There are two commonly used reference frames for inverter controller design: dq rotating (synchronous) reference frame (RRF) [4], [5] and $\alpha\beta$ stationary reference frame (SRF) [6], [7]. In general, RRF-based control scheme uses two pairs of proportional integral (PI) controllers, which situate in two reference frames while rotating in the opposite directions, to regulate positive-sequence (PS) and negative-sequence (NS) components, respectively [4]. However, the RRF-based control strategies need band-stop filters to acquire the DC components of the measurement signals. Adding filters introduce delays that can worsen the dynamic performance of voltage regulation. In [5], Cai *et al*. applied the proportional resonant (PR) controller for NS voltage regulation to avoid the delay caused by the added filter, but it requires high accuracy for the decomposition of PS and NS components.

SRF-based control scheme requires one pair of PR controllers for voltage regulation in AC domain. In [6], [7], the voltage reference is generated by the droop control and an unbalance compensator. The power used in droop control is calculated using PS components so that the unbalance compensator is applied for the reference generation to regulate the NS voltage. However, the proposed control scheme in this paper can achieve NS regulation without the need for the unbalance compensator. Moreover, in the previous works, no output transformer is connected with the inverter. Thus, zero-sequence (ZS) network components are not analyzed and ZS voltage regulation is not considered.

In this paper, to enhance the grid-forming operation of the battery-energy-storage system (BESS) in an islanded microgrid, we propose an $\alpha\beta$ SRF-based control structure for the BESS to regulate the PS and NS voltage while using a grounding transformer (GT) to reduce the ZS voltage. Our contributions are threefold. *First*, we clearly demonstrated the advantages of the SRF-based inner voltage control scheme for PS and NS voltage regulation over the RRF-based control scheme. *Second*, we demonstrated that ZS voltage caused by unbalanced loads can be effectively reduced when adding a GT at the PCC by analyzing the ZS network components. *Third*,

This research is supported by the U.S. Department of Energy's Office of Energy Efficiency and Renewable Energy (EERE) under the Solar EnergyTechnologies Office Award Number DE-EE0008770.

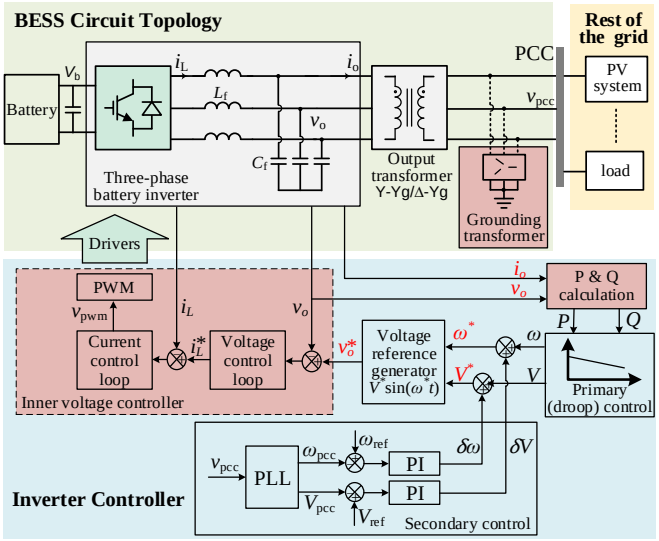

Fig. 1. Topology and control structure of a three-phase grid-forming BESS.

we derived the relationship between power and voltage unbalance and proposed a performance metric for regulating power unbalance to meet inverter voltage unbalance requirements.

II. Voltage Control Strategy

As shown in Fig. 1, a grid-forming BESS consists of a three-phase inverter, an LC filter, and a Y-Yg (or Δ-Yg) isolation transformer for connecting the BESS to the main grid. In [8], Guerrero *et al.* proposed a commonly used droop-based hierarchical control structure, consisting of inner current and voltage control loops, primary (droop) control, and secondary control. This structure allows the seamless transition between the off-grid mode and the grid-connected mode without changing the control algorithm. When working in the off-grid mode, the grid-forming BESS inverter operates as a voltage source with two main functions: regulating PCC voltage, $v_{\rm pcc}$, and setting system frequency, f.

Our contributions to this topology and control scheme are highlighted in red in Fig. 1. First, we designed an $\alpha\beta$ SRF-based inverter controller. The voltage reference of the inner voltage controller, $v_{\rm o}^*$, is generated based on the conventional droop and secondary control without the need for the decomposition of the PS and NS components. The inner voltage controller design for PS and NS voltage regulation is described in Section II-B in detail. Second, we added a GT in the circuit to mitigate the impact of ZS currents on voltage regulation for keeping $v_{\rm pcc}$ balanced when serving highly unbalanced single-phase loads.

A. Positive- and Negative- Sequence Voltage Representation

Unbalanced three-phase phasors can be decomposed into PS, NS, and ZS phasors [4]. The PS and NS voltages are expressed as:

$$\begin{bmatrix} v_a^+ \\ v_b^+ \\ v_c^+ \end{bmatrix} = \begin{bmatrix} V_m^+ \cos(\omega t + \varphi^+) \\ V_m^+ \cos(\omega t - 2\pi/3 + \varphi^+) \\ V_m^+ \cos(\omega t + 2\pi/3 + \varphi^+) \end{bmatrix} \tag{1}$$

$$\begin{bmatrix} v_a^- \\ v_b^- \\ v_c^- \end{bmatrix} = \begin{bmatrix} V_m^- \cos(\omega t + \varphi^-) \\ V_m^- \cos(\omega t + 2\pi/3 + \varphi^-) \\ V_m^- \cos(\omega t - 2\pi/3 + \varphi^-) \end{bmatrix} \tag{2}$$

where V_m^+ and V_m^- are the amplitude of PS and NS voltage, respectively; φ^+ and φ^- are the phase of PS and NS voltage, respectively. By using the Clarke transformation matrix T_1, the voltages in SRF ($\alpha\beta$-coordinate) are obtained:

$$\begin{bmatrix} v_\alpha^+ \\ v_\beta^+ \end{bmatrix} = T_1 \begin{bmatrix} v_a^+ \\ v_b^+ \\ v_c^+ \end{bmatrix} = \begin{bmatrix} V_m^+ \cos(\omega t + \varphi^+) \\ V_m^+ \sin(\omega t + \varphi^+) \end{bmatrix} \tag{3a}$$

$$\begin{bmatrix} v_\alpha^- \\ v_\beta^- \end{bmatrix} = T_1 \begin{bmatrix} v_a^- \\ v_b^- \\ v_c^- \end{bmatrix} = \begin{bmatrix} V_m^- \cos(\omega t + \varphi^-) \\ V_m^- \sin(\omega t + \varphi^-) \end{bmatrix} \tag{3b}$$

where

$$T_1 = \frac{2}{3}\begin{bmatrix} 1 & -1/2 & -1/2 \\ 0 & \sqrt{3}/2 & -\sqrt{3}/2 \end{bmatrix}$$

By using the Clarke-Park transformation matrix T_2, the voltages in RRF (dq-coordinate) are derived:

$$\begin{bmatrix} v_d^+ \\ v_q^+ \end{bmatrix} = T_2 \begin{bmatrix} v_a^+ \\ v_b^+ \\ v_c^+ \end{bmatrix} = \begin{bmatrix} V_m^- \cos\varphi^+ \\ V_m^- \sin\varphi^+ \end{bmatrix} \tag{4a}$$

$$\begin{bmatrix} v_d^- \\ v_q^- \end{bmatrix} = T_2 \begin{bmatrix} v_a^- \\ v_b^- \\ v_c^- \end{bmatrix} = \begin{bmatrix} V_m^- \cos(2\omega t + \varphi^-) \\ -V_m^- \sin(2\omega t + \varphi^-) \end{bmatrix} \tag{4b}$$

where

$$T_2 = \frac{2}{3}\begin{bmatrix} \cos(\omega t) & \cos(\omega t - 2\pi/3) & \cos(\omega t + 2\pi/3) \\ -\sin(\omega t) & -\sin(\omega t - 2\pi/3) & -\sin(\omega t + 2\pi/3) \end{bmatrix}$$

B. Inner Voltage Controller Design

Fig. 2(a) depicts the PS and NS inner voltage controller of the battery inverter in the double synchronously rotating dq reference frames. The three-phase voltages and currents are transformed into PS dq^+ axes and NS dq^- axes voltages and currents using a positive phase-locked-loop (PLL) angle θ and a negative PLL angle $-\theta$, respectively [4].

From (4), it can be seen that although the PS component decomposed to the dq coordinate is DC, the dq projection of the NS component is not DC but a second harmonic (2ω) AC. Thus, monitoring and controlling PS and NS voltages require a dual-reference control scheme, PS dq^+ RRF and NS dq^- RRF, rotating in the opposite direction. In addition, the second harmonics should be filtered or removed from the PS and NS dq-axes quantities before being sent to the PI controllers in the inner current and voltage control loops. Thus, band-stop filters (notch filters) are used to reject double-frequency components while leaving other frequencies components unaltered. However, adding the filter introduces filter delay and slows down the convergence of the output phase angle.

Fig. 2(b) illustrates the inner voltage controller in the SRF. From (3), it can be seen that PS and NS components in $\alpha\beta$ coordinate are AC values with the grid's nominal frequency, $\omega = 2\pi f$. Thus, both voltage and current controllers are based on the PR control instead of the conventional PI control. The advantage of the PR control is that it can provide infinite gain

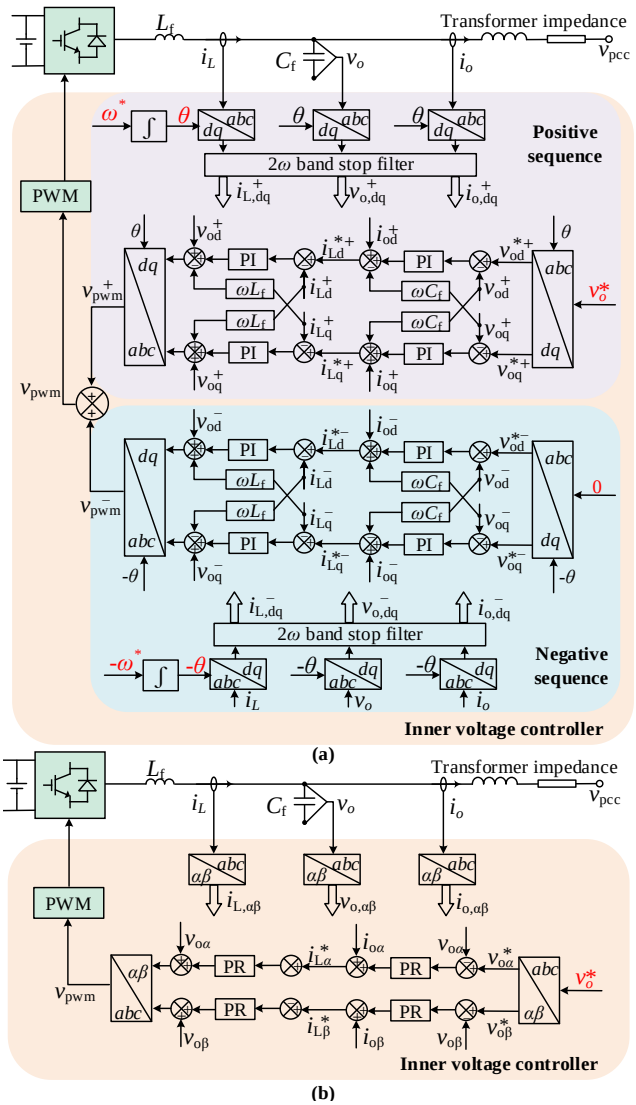

Fig. 2. Control diagram of the inner controller of a three-phase grid-forming BESS inverter. (a) dq RRF-based control; (b) $\alpha\beta$ SRF-based control.

at the selected resonant frequency. Therefore, it has excellent tracking capability of AC variables. Because the inner loops are implemented in two-phase stationary frame and all the measured voltage and current are directly transformed from abc to $\alpha\beta$ coordinates, the computational burden is greatly simplified.

In Section III-A, we will conduct a side-by-side performance comparison to demonstrate the advantage of using the $\alpha\beta$ SRF based control structure.

C. Output Transformer Configuration Design

When serving unbalanced loads in power distribution grids, apart from the PS and NS components, ZS components are another contributor to the unbalanced voltage. The ZS circuit of a BESS is determined mainly by the output transformer characteristics, such as the connection method of the primary and secondary windings, the winding grounding arrangements, and the construction type of the magnetic circuit.

The output transformers for IBRs have two connection types: Y-Yg (see Fig. 3(a)) and Δ-Yg (see Fig. 3(b)) [9]. The

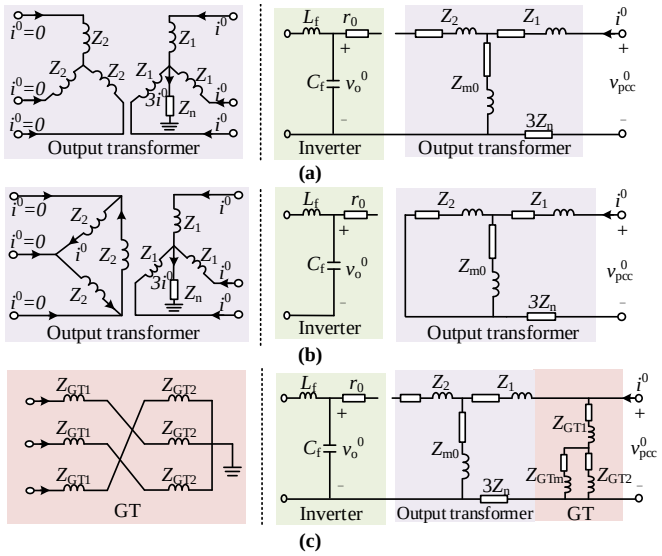

Fig. 3. Zero-sequence equivalent circuit. (a) With Y-Yg output transformer; (b) With Δ-Yg output transformer; (c) With Y-Yg output transformer and GT.

ZS impedance of a Y-Yg transformer, $Z^0_{\mathrm{Y-Y_g}}$, and a Δ-Yg transformer, $Z^0_{\Delta-\mathrm{Y_g}}$, can be expressed as:

$$Z^0_{\mathrm{Y-Y_g}} = Z_1 + Z_{\mathrm{m0}} + 3Z_{\mathrm{n}} \approx Z_{\mathrm{m0}} \tag{5}$$

$$\begin{aligned} Z^0_{\Delta-\mathrm{Y_g}} &= Z_1 + (Z_2 // Z_{\mathrm{m0}}) + 3Z_{\mathrm{n}} \\ &\approx Z_1 + Z_2 + 3Z_{\mathrm{n}} \end{aligned} \tag{6}$$

where $Z_{\mathrm{m0}} = r_{\mathrm{m0}} + j\omega L_{\mathrm{m0}}$ is the transformer magnetizing impedance, Z_{n} is the grounding impedance, $Z_1 = r_1 + j\omega L_1$ and $Z_2 = r_2 + j\omega L_2$ are the primary and secondary transformer impedance, respectively.

From (5) and (6), it can be seen that $Z^0_{\mathrm{Y-Y_g}} \gg Z^0_{\Delta-\mathrm{Y_g}}$ because the magnetizing impedance is thousands of times higher than transformer winding impedance and grounding impedance by design. Thus, the ZS voltage and current in a system with a Y-Yg output transformer would be higher than those with a Δ-Yg output transformer. However, because Δ-Yg transformer configuration provides the additional ZS path, upstream relays might not trip during the ground fault. Thus, Δ-Yg configuration should not be used in most ground-connected distribution networks [10].

To reduce the ZS voltage at the PCC when using a Y-Yg output transformer, we propose to add a GT (Δ-Yg or Zig-Zag configuration) to the PCC (See Fig. 1). As shown in Fig. 3(c), by providing the ZS current with a low-impedance path to flow through, the ZS impedance, $Z^0_{\mathrm{Y-Y_g/GT}}$, is:

$$\begin{aligned} Z^0_{\mathrm{Y-Y_g/GT}} &= (Z_{\mathrm{GT1}} + Z_{\mathrm{GTm}} // Z_{\mathrm{GT2}})) // (Z_{\mathrm{m0}} + 3Z_{\mathrm{n}} + Z_1) \\ &\approx Z_{\mathrm{GT1}} + Z_{\mathrm{GT2}} \end{aligned} \tag{7}$$

where Z_{GT1}, Z_{GT2}, Z_{GTm} are the primary, secondary, and magnetizing impedance of the GT, respectively. As Z_{GT} is much smaller than Z_{m0}, the ZS voltage at the PCC can be significantly reduced.

From Fig. 3, we can see that ZS current cannot flow in the three-wire ungrounded inverter, so the inverter inner voltage

TABLE I
SIMULATION PARAMETERS

Inverter Electrical Parameters	
System Frequency f	60 Hz
PCC Nominal Voltage $v_{\rm pcc}$ (line-line)	4160 $V_{\rm rms}$
Inverter Nominal Voltage $v_{\rm o}$ (line-line)	480 $V_{\rm rms}$
Battery Nominal Voltage $V_{\rm b}$	1200 V
LC Filter Inductance $L_{\rm f}$	350 µH
LC Filter Inductance $C_{\rm f}$	5000 µF
Inverter Controller Parameters	
Current PR controller Proportional gain $k_{\rm pi}$	4
Current PR controller Resonant gain $k_{\rm ri}$	200
Voltage PR controller Proportional gain $k_{\rm pv}$	2
Voltage PR controller Resonant gain $k_{\rm rv}$	1000
Droop controller Coeff. $n_{\rm p}$, $n_{\rm q}$	$1e^{-7}$
Secondary freq. PI controller gain $k_{\rm 2pf}$, $k_{\rm 2if}$	0.3, 10
Secondary voltage PI controller gain $k_{\rm 2pv}$, $k_{\rm iv}$	0.001, 0.5
Output Transformer Parameters	
Nominal Power, frequency	5 MVA, 60Hz
Nominal Voltage (line-line)	480 $V_{\rm rms}$ / 4160 $V_{\rm rms}$
Resistance r_1 r_2, leakage inductance L_1 L_2	0.0012 p.u., 0.03 p.u.
Magnetization impedance $r_{\rm m}$, $L_{\rm m}$	200 p.u., 200 p.u.
Core type	Three-limb core

controller cannot sense and regulate the ZS components at the PCC by design. Thus, adding a GT to reduce the ZS voltage at the PCC is the best option for maintaining balanced $v_{\rm pcc}$. Note that adding a GT also provides an effective grounding for the BESS during ground faults.

III. SIMULATION RESULTS ANALYSIS

To verify the performance of the proposed unbalance voltage control scheme, an electromagnetic transient (EMT) microgrid testbed for the IEEE 123-bus distribution feeder system was developed on the OPAL-RT platform. A 2-MVA BESS with the topology shown in Fig. 1 is connected at the feeder head (i.e., Node 149). The BESS is the only grid-forming resource in the microgrid. To test the BESS operation in two operation conditions: supplying and absorbing unbalanced power, we add a 5-MVA, grid-following PV system (parameters given in [11]) to the feeder at node 149. The electrical and controller parameters of the BESS modeled on OPAL-RT/eMEFASIM are listed in Table I. The GT is designed based on IEEE 1547.8 standard [12] (rated at 3.772 MVA with ZS impedance of 0.6185 p.u.).

A. Performance Comparison between the SRF and RRF based Controller Design Methods

We compare the controller performance of the proposed $\alpha\beta$ SRF-based method with the conventional dq RRF-based method. As shown in Fig. 4, initially, the BESS operates in battery discharging mode with unbalanced output three-phase current ($I_{\rm A} = 0.1$ p.u., $I_{\rm B} = 0.6$ p.u., $I_{\rm C} = 0.3$ p.u.). At $t = 1$s, an unbalanced load step change is applied so that the BESS absorbs power from the grid at phase a and c ($I_{\rm A} = -0.4$ p.u. and $I_{\rm C} = -0.1$ p.u.) and supplies power to the grid at phase b ($I_{\rm B} = 0.2$ p.u.).

The steady-state value of PCC voltage and current are the same in both cases, which indicates that both control schemes have a good current tracking performance in steady-state.

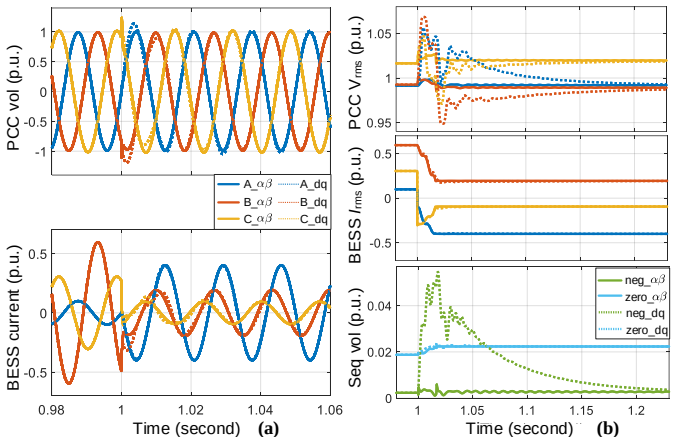

Fig. 4. Performance comparison of $\alpha\beta$-based and dq-based control methods. (a) Time-series waveforms of PCC voltage and current; (b) RMS profiles of PCC voltage and BESS current, and NS and ZS components of PCC voltage

However, the dynamic performance of the proposed $\alpha\beta$ SRF-based control scheme is significantly better than that of the dq RRF-based method. As shown in Fig. 4(b), when taking the RRF-based approach, the NS voltage overshoots and it takes 200 ms to damp. As a result, the PCC voltage can overshoot above 1.05 p.u. and the unbalance of the three-phase voltage is significant in the 200-ms period. The results demonstrate that because no filters are required when using the SRF-based approach, its voltage tracking performance outperforms the RRF-based approach.

B. Power-Voltage Unbalance Curves

Voltage unbalance factor (VUF) and power unbalance factor (PUF) are commonly used to quantify voltage and load power unbalance. The definitions of VUF can be found in standards, such as [12]–[14]. Most standards require electrical supply systems to be designed for limiting the maximum voltage unbalance to 3%. As introduced in [15], when considering ZS voltage in four-wire system, VUF is calculated as:

$$VUF = \sqrt{V_-^2 + V_0^2}/|V_+| \tag{8}$$

where V_+, V_-, and V_0 are the magnitude of PS, NS and ZS voltage. In this paper, we calculate PUF as:

$$PUF = \frac{Max(|P_{\rm A} - P_{\rm avg}|, |P_{\rm B} - P_{\rm avg}|, |P_{\rm C} - P_{\rm avg}|)}{|P_{\rm rated}|} \tag{9}$$

where $P_{\rm A/B/C}$ represents the power magnitude of phase $a/b/c$, $P_{\rm avg} = (P_{\rm A} + P_{\rm B} + P_{\rm C})/3$ is the three-phase power average, and $P_{\rm rated}$ is the rated power per phase.

Experiments can be conducted for different PUF values so that the corresponding VUF points can be computed. Then, a PUF-UVF curve can be obtained, as shown in Fig. 5. From the figure, we can see that the VUF of the Δ-Yg output transformer is very linear and when PUF increases from 0 to 0.65, the VUF can be maintained below 1%. However, if a Y-Yg output transformer is used, VUF can be regulated within 3% only when PUF is 30% or less. If a GT is added to the Y-Yg output transformer, VUF can be regulated within 3% when PUF 55% or less, a significant improvement to the system

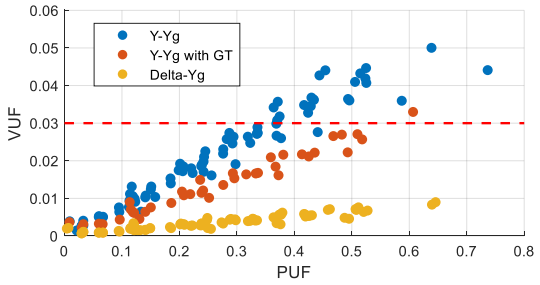

Fig. 5. PUF versus VUF for different transformer configurations

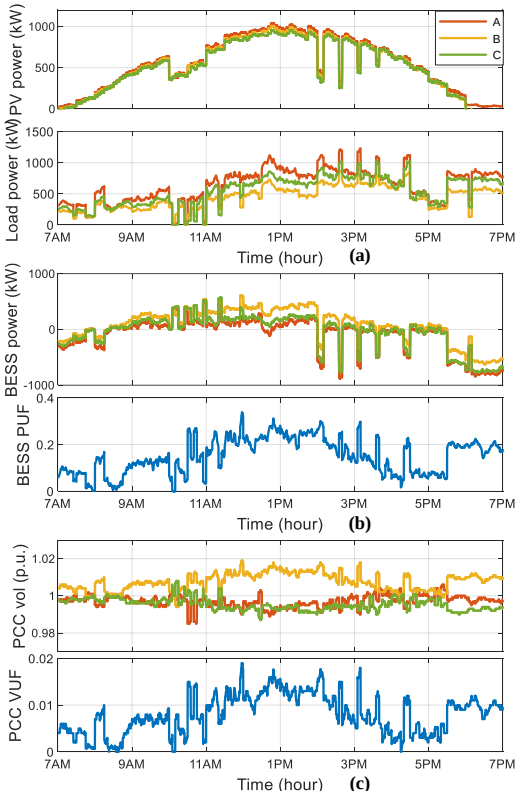

Fig. 6. Real-time simulation results for the IEEE 123-bus testbed. (a) PV and load power; (b) BESS output power and PUF; (c) PCC voltage and VUF

capability of supplying unbalanced loads. The importance of the PUF-VUF curve is that it reveals the power unbalance limit, which can be used by an energy management system as an operational constraint for maintaining power balance.

C. Real-time Simulation Results

The proposed control scheme for mitigating voltage unbalance is verified on the real-time simulator, OP5700-OPAL-RT, with a 12-hour simulation from 7:00 am to 7:00 pm. The model in OPAL-RT is sampled at every 100us. As shown in Fig. 6(a), the PV and load power scheduling are based on the energy management algorithm in [16], where PV curtailment and load shedding are executed to meet the power supply needs. Because PUF (see Fig. 6(b)) was maintained below 55%, VUF (see Fig. 6(c)) was within 3%. Note that PUF and VUF have similar shapes. This is because the PUF-VUF curve is close to linear when adding a GT to the Y-Yg output transformer, as shown by the red dots in Fig. 5.

IV. Conclusion

In this paper, we propose an $\alpha\beta$ SRF-based voltage unbalance control architecture for a grid-forming BESS. Compared with the dq RRF-based approach, the proposed method eliminates band-stop filters and achieves superior tracking capabilities. We propose to include a GT at the PCC to further reduce the system voltage unbalance. We derive the PUF-VUF curves for different transformer configurations. This allows the power unbalanced limits to be calculated from the inverter voltage unbalance limits for microgrid power management purposes. The simulation results demonstrate that when using the proposed SRF-based inner voltage control loop and adding a GT with the Y-Yg connected output transformer, VUF can be regulated within 3% when the PUF is limited within 55%.

References

[1] A. Hooshyar and R. Iravani, "Microgrid protection," *Proceedings of the IEEE*, vol. 105, no. 7, pp. 1332–1353, 2017.

[2] I. Vechiu, O. Curea, and H. Camblong, "Transient operation of a four-leg inverter for autonomous applications with unbalanced load," *IEEE Transactions on Power Electronics*, vol. 25, no. 2, pp. 399–407, 2009.

[3] X. Zhang and J. Wang, "Research on phase-locked control strategy for three-phase combined inverters," in *2009 Third International Conference on Genetic and Evolutionary Computing*. IEEE, 2009, pp. 260–263.

[4] N. Tleis, *Power systems modelling and fault analysis: theory and practice*. Elsevier, 2007.

[5] H. Cai, P. Zhang, H. Zhao, J. Shi, W. Yao, and X. He, "Controller design for three-phase inverter with power unbalanced loads applied in microgrids," in *2015 IEEE Energy Conversion Congress and Exposition (ECCE)*. IEEE, 2015, pp. 4588–4593.

[6] M. Savaghebi, A. Jalilian, J. C. Vasquez, and J. M. Guerrero, "Autonomous voltage unbalance compensation in an islanded droop-controlled microgrid," *IEEE Transactions on Industrial Electronics*, vol. 60, no. 4, pp. 1390–1402, 2012.

[7] X. Zhao, X. Wu, L. Meng, J. M. Guerrero, and J. C. Vasquez, "A direct voltage unbalance compensation strategy for islanded microgrids," in *2015 IEEE Applied Power Electronics Conference and Exposition (APEC)*. IEEE, 2015, pp. 3252–3259.

[8] J. M. Guerrero, J. C. Vasquez, J. Matas, L. G. De Vicuña, and M. Castilla, "Hierarchical control of droop-controlled ac and dc microgrids—a general approach toward standardization," *IEEE Transactions on industrial electronics*, vol. 58, no. 1, pp. 158–172, 2010.

[9] R. Aboelsaud, A. Ibrahim, and A. G. Garganeev, "Review of three-phase inverters control for unbalanced load compensation," *International Journal of Power Electronics and Drive Systems*, vol. 10, no. 1, p. 242, 2019.

[10] A. Vukojevic and S. Lukic, "Microgrid protection and control schemes for seamless transition to island and grid synchronization," *IEEE Transactions on Smart Grid*, vol. 11, no. 4, pp. 2845–2855, 2020.

[11] V. Paduani, H. Yu, B. Xu, and N. Lu, "A unified power-setpoint tracking algorithm for utility-scale pv systems with power reserves and fast frequency response capabilities," *IEEE Transactions on Sustainable Energy*, pp. 1–1, 2021.

[12] "IEEE draft recommended practice for establishing methods and procedures that provide supplemental support for implementation strategies for expanded use of ieee standard 1547," *IEEE P1547.8/D8, July 2014*, pp. 1–176, 2014.

[13] "IEEE recommended practice for monitoring electric power quality," *IEEE Std 1159-2009 (Revision of IEEE Std 1159-1995)*, pp. 1–94, 2009.

[14] "Motors and generators," *NEMA Standard MG1-1993, NEMA Std.*, 1993.

[15] F. Shahnia, P. J. Wolfs, and A. Ghosh, "Voltage unbalance reduction in low voltage feeders by dynamic switching of residential customers among three phases," *IEEE Transactions on Smart Grid*, vol. 5, no. 3, pp. 1318–1327, 2014.

[16] R. Hu, Y. Li, S. Zhang, A. Shirsat, V. Muthukaruppan, W. Tang, M. Baran, D. Lubkeman, and N. Lu, "A load switching group based feeder-level microgrid energy management algorithm for service restoration in power distribution system," *arXiv preprint arXiv:2011.08735*, 2020.